Bistable emission of a black-body radiator

S. M. Redmond and S. C. Rand[a)]
Department of Electrical Engineering and Computer Science, University of Michigan,
Ann Arbor, Michigan 48109

S. L. Oliveira
Instituto de Fisica de Sao Carlos, Universidade de Sao Paulo, CP 369 CEP 13560-970,
Sao Carlos-SP, Brazil

Bistable black-body emission is reported from resonantly excited $Er^{3+}, Yb^{3+}:Y_2O_3$ nanopowders. A simple model based on thermo-optic nonlinear response in the strongly scattering random medium explains the observed behavior. © *2004 American Institute of Physics.* [DOI: 10.1063/1.1825068]

Bistability is common in nonlinear dynamical systems, but there have been no reports of intrinsic instabilities in black-body emission of optically excited media.[1] Intrinsically bistable photo-luminescence has been reported however in Yb-doped heavy metal halide crystals[2,3] at cryogenic temperatures and also in room temperature experiments in rare-earth-doped laser glass[4] and transition metal laser hosts.[5] Since thermal conduction and reflectivity play key roles in the internal heat balance thought to influence luminescent instabilities, we investigated laser crystals prepared as nanopowders to see if their altered transport properties might lead to more pronounced instabilities at high temperatures. $Yb^{3+}:Y_2O_3$ is an example of a laser material currently under development for compact, high-power *ceramic* lasers, where multiple scattering and attendant luminescent instabilities could restrict designs or impair performance. The rapid spectral quenching of visible luminescence and the abrupt appearance of high-temperature black-body radiation in $Er^{3+}, Yb^{3+}:Y_2O_3$ nanopowders reported in this letter indicate that fundamental scaling limits may indeed exist in ceramic[6] and random lasers.[7] These phenomena also enhance laser processing of ceramics and reflective metals.

Rare-earth-doped powders were prepared for these experiments by flame spray pyrolysis, and consisted of unaggregated single-crystal particles with average diameters in the range of 10–200 nm.[8] Transmission experiments with free-standing samples pressed lightly into wedges of 1 mm maximum thickness were used to determine the Yb^{3+} absorption coefficient in the presence of multiple scattering. Disks with measured filling fractions of 15–20% were mounted at the entrance of an integrating sphere and transmission of a laser beam was measured versus sample thickness as shown in Fig. 1, where the $^2F_{7/2}(0) - ^2F_{5/2}(2')$ infrared absorption resonance of Yb is evident. A direct comparison of attenuation on and off resonance, together with the data in the inset of Fig. 1, showed that the absorption length of the sample at $\lambda = 905.6$ nm was $\ell_\alpha = 0.505$ mm. (This value was more than an order of magnitude less than the absorption length of an equal concentration of Yb ions in crystalline Y_2O_3. For an impurity density of $N^{Yb} = 4.1 \times 10^{20}$ cm^{-3} and a cross section of $\sigma = 0.35 \times 10^{-20}$ cm^2,[9] the calculated absorption length is $\ell'_\alpha = 7.0$ mm at zero porosity.) With low absorption and high reflectivity $(R > 96\%)$ an incident power of 400 mW tuned to the Yb resonance leads to a total absorbed power of at

most 14 mW in a 1 mm thick sample, even when multiple scattering is taken into account. Hence, from the outset, strong thermal interactions are not anticipated at the surface of such weakly absorbing samples with high albedo.

In view of this, the difference between the emission spectra of an $Er^{3+}, Yb^{3+}:Y_2O_3$ powder sample irradiated at two different laser powers (Fig. 2) is quite remarkable. At an input power of 250 mW, visible emission originates principally from the $^2H_{11/2}$ multiplet, whereas at 50 mW it originates almost entirely from $^4S_{3/2}$. Yet both emission spectra result from the same basic process of upconversion,[10] involving infrared absorption by two Yb^{3+} ions followed by energy transfer to the $^4F_{7/2}$ level of the secondary dopant ion Er^{3+}. In $Er^{3+}, Yb^{3+}:CsCdBr_3$, thermally activated upconversion can result in abrupt switching of luminescent spectra.[11] Here, in $Er^{3+}, Yb^{3+}:Y_2O_3$ nanopowder, we find that a remarkably sudden, thermally induced spectral change of different origin is observed. First, the $^4F_{7/2}$ population is rapidly transferred to the $^4S_{3/2}$ state in the Y_2O_3 host through resonant cross relaxation.[10] Hence, emission normally originating from the $^4S_{3/2}$ state at room temperature produces thermally activated $^2H_{11/2}$ emission at higher temperatures. This occurs above 1162 K, when thermal energies exceed the $^4S_{3/2} - ^2H_{11/2}$ intermanifold energy splitting of 807 cm^{-1} (see Fig. 3 inset), and the $^2H_{11/2}$ state becomes significantly populated. Sample emission changes color. Second, with further increases of input power (additional laser heating), visible luminescence from the sample virtually disappears—it is strongly quenched over a wide interval of pump power. Finally, at the
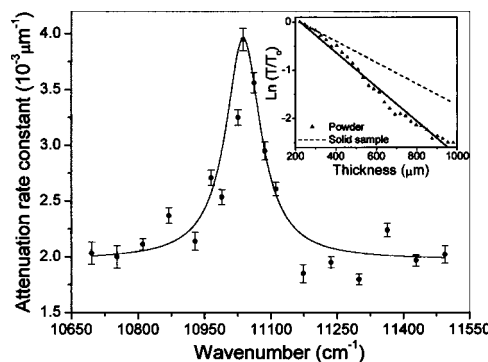

FIG. 1. Absorption spectrum of $Yb^{3+}, Er^{3+}:Y_2O_3$, in the region of the $^2F_{7/2} - ^2F_{5/2}$ transition, showing increased attenuation on the Yb resonance. The solid curve is a Gaussian best fit. Inset: Logarithm of transmission vs thickness measured through a lightly pressed free-standing powder layer.

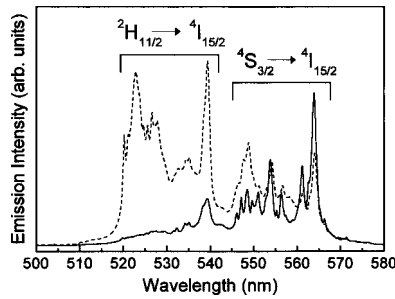[a)]Electronic mail: scr@eecs.umich.edu

FIG. 2. Luminescence spectra of $Er^{3+}, Yb^{3+}:Y_2O_3$ nanopowder at two incident intensities: Low power (50 mW, solid) and high power (250 mW, dashed). Excitation wavelength was $\lambda_{ex} = 905.6$ nm.

highest available input intensities, broadband emission arises. (Fig. 3, extreme right).

In the low-power regime of Fig. 3 below 100 mW, luminescent intensity rises quadratically as expected for a two-photon process.[11] Above this value, however, it undergoes an abrupt reversal. Luminescence is strongly quenched. As the incident intensity is increased further, between 150 mW and 400 mW, all transitions steadily *decrease in intensity*. Data in Fig. 3 were taken at $\lambda_{em} = 522.4$ nm under steady-state temperature conditions, using an intensity-stabilized Ti:Sapphire laser and scanning times of 0.5 h or more. The behavior of fluorescence versus incident power was virtually identical on all Yb and Er transitions.

A model combining heat transfer and population rate equations predicts the essential features of this complex emission behavior. Equation (1) relates the sample temperature to the input intensity I_i (corrected for reflectivity R at the input), by balancing energy input with losses from thermal conduction, impurity emission, and black-body radiation. The first term on the right is the thermal conduction loss rate, proportional to the difference between sample temperature T and reference T_0 (295 K) through the thermal conductivity κ and a geometric factor χ. The second term describes resonance fluorescence with a quantum efficiency of $Q(T) = \gamma_{21}/[\gamma_{21} + \gamma_{nr}(T)]$, where γ_{21} is the radiative rate and γ_{nr} is the nonradiative decay rate from level 2 to level 1. The third term is the radiant loss from black-body emission, where σ is the Stefan–Boltzmann constant and A is the irradiated area. The last term accounts for black-body emission that is reabsorbed by Er impurities (see right inset Fig. 4). Equation (1) was augmented by rate equations for the populations $N_i^{Yb}(T)$ and $N_j^{Er}(T)$ of Yb and Er energy levels i and j, respectively
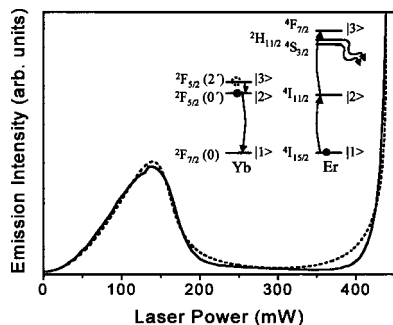

FIG. 3. Luminescence intensity measured at $\lambda = 522.4$ nm vs input power, together with the predicted emission intensity I_{theory} (dashed curve). A quadratic increase in upconversion intensity is evident below 100 mW, followed by spectral quenching in the region between 150–350 mW, and continuum generation above 375 mW.
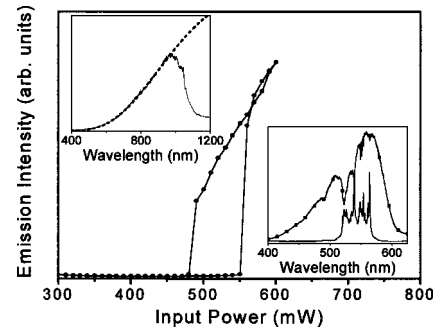

FIG. 4. Black-body emission intensity vs pump power ($1/e^2$ spot diameter $\phi = 75$ μm). In the main plot, the lower (upper) branch of the hysteresis loop corresponds to increasing (decreasing) power. Left inset: White-light emission spectrum, corrected for instrumental response. For $\lambda > 1$ μm, photomultiplier sensitivity drops to zero; background is from overlapping spectral orders. The dashed curve is a Planck distribution fit ($T = 1910$ K). Right inset: Uncorrected white-light emission spectrum showing large resonant reabsorption features due to ground-state Er ions.

$(i, j = 1, 2, 3)$. Only energy transfer involving the long-lived excited state $|2\rangle$ of Yb was considered and two-photon energy transfer upconversion[11] was assumed to populate luminescent Er level $|3\rangle$.

$$(1 - R(T))I_i = \kappa(T)[T - T_0]\chi + (1 - R(T))I_i \frac{\nu_{em}}{\nu_o}Q(T)$$
$$+ \sigma A[T^4 - T_0^4] - \alpha_\nu I_\nu(T), \tag{1}$$

$$\dot{N}_1^{Yb} = -BI_iN_1^{Yb} + \gamma_2^{Yb}(T)N_2^{Yb} + \gamma_{31}^{Yb}N_3^{Yb}, \tag{2}$$

$$\dot{N}_2^{Yb} = \gamma_{32}^{Yb}N_3^{Yb} - \Gamma_{21}N_2^{Yb}N_1^{Er} - \Gamma_{22}N_2^{Yb}N_2^{Er} - \gamma_2^{Yb}(T)N_2^{Yb}, \tag{3}$$

$$\dot{N}_3^{Yb} = BI_iN_1^{Yb} - \gamma_3^{Yb}N_3^{Yb}, \tag{4}$$

$$\dot{N}_1^{Er} = -\Gamma_{21}N_2^{Yb}N_1^{Er} + \gamma_{21}^{Er}N_2^{Er} + \gamma_{31}^{Er}N_3^{Er}, \tag{5}$$

$$\dot{N}_2^{Er} = \gamma_{32}^{Er}N_3^{Er} + \Gamma_{21}N_2^{Yb}N_1^{Er} - \Gamma_{22}N_2^{Yb}N_2^{Er} - \gamma_{21}^{Er}N_2^{Er}, \tag{6}$$

$$\dot{N}_3^{Er} = \Gamma_{22}N_2^{Yb}N_2^{Er} - \gamma_3^{Er}N_3^{Er}. \tag{7}$$

In Eqs. (1)–(7), B is the usual Einstein stimulated absorption coefficient. I_ν is the black-body specific intensity given by Planck's law, and α_ν is the Er ground state absorption coefficient at frequency ν.

In Fig. 3, the theoretical curve is given by $I_{theory} = I_\nu^{Er} + I_\nu(T)$. It contains contributions from Er impurities ($I_\nu^{Er} = N_3^{Er}\gamma_3^{Er}h\nu$, where $\gamma_3^{Er} = \gamma_{32}^{Er} + \gamma_{31}^{Er}$) and black-body radiation [$I_\nu(T)$]. Yb^{3+} has no visible emission and therefore does not contribute to the signal. The temperature-dependent decay rate $\gamma_2^{Yb}(T) = \gamma_{21}^{Yb} + \gamma_{nr}^{Yb}(T)$ was measured with time-resolved photoluminescence over an extended temperature range, from 300 to 1200 K.[12] Thermal conductivity values over the same range were obtained from Ref. 13. Rate constants Γ_{kl}, the energy transfer rates on coupled transitions for Yb and Er ions initially in states k and l, respectively, were taken to be constants. Explicit temperature dependences of these quantities have not been reported. Reabsorption of black-body radiation by Er was approximated by ($\alpha_\nu I_\nu(T)$), considering only ground-state absorption of Er levels $|2\rangle$ & $|3\rangle$ with α_ν used as a fitting parameter.

Appl. Phys. Lett., Vol. 85, No. 23, 6 December 2004

Redmond, Rand, and Oliveira   5519

Steady-state populations $N_i(T)$ $(i=1,2,3)$ were found by setting $\dot{N}_i^{\text{Yb}}=\dot{N}_j^{\text{Er}}=0$ and using closure $(N_1^{\text{Er}}+N_2^{\text{Er}}+N_3^{\text{Er}}=N^{\text{Er}};N_1^{\text{Yb}}+N_2^{\text{Yb}}+N_3^{\text{Yb}}=N^{\text{Yb}})$. The result for the highest Er level is $N_3^{\text{Er}}(T)=2\Gamma_{23}\Gamma_{12}(BI)^2N_1^{\text{Er}}(N_2^{\text{Yb}})^2/\gamma_{21}^{\text{Er}}\gamma_{31}^{\text{Er}}(\gamma_{21}^{\text{Yb}}(T))^2=cI^2/(\gamma_{21}^{\text{Yb}}(T))^2$, where c is a constant in the undepleted pump approximation. The temperature dependence of Er decay constants was ignored in fitting the data of Fig. 3. This assumption is not strictly justified at low incident intensities (low temperatures) where the measured emission is almost entirely due to Er. However, at intermediate to high input powers (medium to high temperatures), strong luminescence quenching renders the Er contribution to the measured emission negligible. Its temperature dependence is therefore much less important than that of the donor ion Yb over most of the experimental range. With only three fitting parameters χ, α_ν, c, the model accounts surprisingly well for the spectral quenching of upconversion luminescence in the left half of Fig. 3. It also predicts the dramatic rise in black-body emission in the right half of the figure, and bistability of this radiation, as detailed below. The spectral variations in Fig. 2 are accounted for separately by thermal activation of $^4S_{3/2}$ impurities to the $^2H_{11/2}$ level, which has forty times the oscillator strength of the $^4S_{3/2}$ level,[14] and will not be discussed further here.

Assuming constant values for α_ν and R, the specific emission intensity is predicted to rise abruptly above input powers of 350 mW (dotted curve in Fig. 3). This corresponds well with the sudden appearance of bright white light in experiments. The intensity rise is symptomatic of a runaway heating process that generates intense visible black-body emission. The experimental white-light spectrum (left inset, Fig. 4) was recorded with achromatic optics and corrected for instrumental response with a standard lamp. The dashed line reveals excellent agreement with a Planck spectrum at $T=(1910\pm10)$ K out to the long-wavelength cutoff of the photomultiplier near 950 nm. The right inset shows resonant reabsorption features of the ground-state Er ions that are comparatively large in the cool wings of illuminated spots, corresponding to the black-body reabsorption term in Eq. (1). Since there are very few Er ions present within one mean transport distance $(\ell^*<0.5~\mu\text{m})$[15] of the surface to account for the strength of the impurity reabsorption, we conclude that (provided melting has not taken place) radiation trapping and absorption enhancement by strong scattering must play a significant role in the mechanism of the optical instability described next.

As shown by the main curve in Fig. 4, the black-body emission shows hysteresis and bistability near the melting point (2410 °C for yttria). Experimentally, upper and lower branch emission intensities were found to be stable for periods exceeding 4 h. Consequently, it seems unlikely that the solid–liquid phase transition could account for the sudden alteration in heat balance, nonlinear temperature rise, and bistability observed in these experiments. On the other hand, melting was confirmed with electron microscopy after irradiation at powers only slightly greater than those necessary to achieve bistability.[16] So, while the model can reproduce the hysteresis accurately based on Er reabsorption of black-body radiation, it also predicts bistability if the reflectivity (or thermal conductivity) decreases by as little as 1% (25%) over a 400 °C range in the premelting zone. Hence, while it seems unlikely that the melting transition *coincides* with bi-

stability, we cannot rule out its influence altogether.

This work shows that luminescence quenching can lead to a thermal runaway process and black-body radiation that exhibits bistability over a small range of input power. Quenching is the result of thermally activated nonradiative decay, whereas the bistable black-body emission is ascribed to nonlinear reabsorption. As yet, no bistability of the rare-earth luminescence itself has been found in powdered $\text{Er}^{3+},\text{Yb}^{3+}:\text{Y}_2\text{O}_3$ over the intensity range where impurity luminescence quenching is first initiated. However at higher input powers, intense black-body radiation is generated that exhibits hysteresis as sample temperatures approach the melting point of yttria. The evidence we have suggests that the optical instability is intrinsic, resulting from the thermal shift $(\lambda_{\text{max}}\sim1/T)$ of the black-body emission spectrum, which increases the absorption as temperature rises. This differs from the shift of the absorption spectrum reported in previous studies of bistable luminescence.[3] In this picture, hysteresis takes place below the melting transition as the result of nonlinear reabsorption of black-body emission by ground-state Er ions. Reflectivity and thermal conductivity fluctuations below the melting transition may also contribute. The dramatic heating effects we have observed can facilitate low-power laser processing of high-temperature ceramics despite the high albedo of powder precursors.[16] Machining of highly reflective metals can also be performed at one-tenth of the normal power levels using a thin nanopowder overlayer to initiate Nd:YAG laser drilling of aluminum plates.[17]

[1] J. Costa, P. Roura, J. R. Morante, and E. Bertran, J. Appl. Phys. **83**, 7879 (1998).

[2] M. P. Hehlen, H. U. Gudel, Q. Shu, J. Rai, S. Rai, and S. C. Rand, Phys. Rev. Lett. **73**, 1103 (1994).

[3] D. R. Gamelin, S. R. Luthi, and H. U. Gudel, J. Phys. Chem. B **104**, 11045 (2000).

[4] A. Kuditcher, M. P. Hehlen, C. M. Florea, K. W. Winick, and S. C. Rand, Phys. Rev. Lett. **84**, 1898 (2000).

[5] M. A. Noginov, B. D. Lucas, and M. Vondrova, J. Opt. Soc. Am. B **19**, 1999 (2002).

[6] J. Lu, J. Lu, T. Murai, K. Takaichi, T. Uematsu, J. Xu, K. Ueda, H. Yagi, T. Yanagitani, and A. A. Kaminskii, Opt. Lett. **27**, 1120 (2002).

[7] N. M. Lawandy, R. M. Balachandran, A. S. L. Gomes, and E. Sauvain, Nature (London) **368**, 436 (1994).

[8] R. M. Laine, T. Hinklin, G. Williams, and S. C. Rand, J. Metastable Nanocryst. Mater. **8**, 500 (2000).

[9] L. Laversenne, Y. Guyot, C. Goutaudier, M. T. Cohen-Adad, and G. Boulon, Opt. Mater. (Amsterdam, Neth.) **16**, 475 (2001).

[10] F. Auzel, Proc. IEEE **61**, 758 (1973).

[11] S. M. Redmond and S. C. Rand, Opt. Lett. **28**, 173 (2003).

[12] S. M. Redmond, Ph.D. dissertation, University of Michigan, 2003.

[13] Y. S. Touloukian, R. W. Powell, C. Y. Ho, and P. G. Klemens, *Thermophysical Properties of Matter*, Thermophysical Properties Research Center Data Series Vol. 2, Thermal conductivity—Nonmetallic solids (IFI-Plenum, New York, 1970), pp. 240–241.

[14] C. A. Morrison, R. P. Leavitt, J. B. Gruber, and N. C. Chang, J. Chem. Phys. **79**, 4758 (1983).

[15] G. R. Williams, S. B. Bayram, S. C. Rand, T. Hinklin, and R. M. Laine, Phys. Rev. A **65**, 013807 (2001).

[16] S. Redmond, S. C. Rand, X. Ruan, and M. Kaviany, J. Appl. Phys. **95**, 4069 (2004).

[17] S. Das (private communication).